Synthesis of Silver Nanoparticle by using *Cassia auriculata* Leaf Powder and its Antibacterial Studies

M. Prem Nawaz, M. Palanivelu, A. Afroos Banu, K. Mohamed Faizal, D. Saravanakkumar and A. Ayeshamariam

Research Journal of Agricultural Sciences
An International Journal

P- ISSN: 0976-1675
E- ISSN: 2249-4538

Volume: 13
Issue: 01

Res. Jr. of Agril. Sci. (2022) 13: 012–017

CARAS

Res. Jr. of Agril. Sci. (Jan-Feb 2022)
13(1): 012–017

ISSN: 0976-1675 (P)
ISSN: 2249-4538 (E)

www.rjas.org

Full Length Research Article

Synthesis of Silver Nanoparticle by using *Cassia auriculata* Leaf Powder and its Antibacterial Studies

M. Prem Nawaz[1], M. Palanivelu[2], A. Afroos Banu[3], K. Mohamed Faizal[4], D. Saravanakkumar[5] and A. Ayeshamariam*[6]

Received: 02 Oct 2021 | Revised accepted: 01 Dec 2021 | Published online: 03 Jan 2022

A B S T R A C T

Herbal nutritional assisted nanoparticles synthesis has a wide range of applications of emerging non-side effect medicinal drugs in recent trends of nano drug research as far as being based with ecofriendly. Phytochemicals of traditional herbal namely Cassia auriculata leaf's intermediated Silver (Ag) nanoparticles (NPs) have been synthesized in employing ultra sound effect so called Sonochemical techniques. In this present work on green synthesis approach, one of the best candidates, Ag nanoparticles act as potential agent to investigate the antibacterial activity by well diffusion method. The essential role of crystal size of NPs on both antimicrobial and heavy metal absorption and other relevant primary crystallographic data is derived by the powder x-ray diffraction (PXRD) crystallography cornerstone rapid analytic technique. Its result revealed the formation of Ag nanostructure along with prepared samples. Optical outcomes like absorption and transmittance for part of the electromagnetic spectrum as well as the functional vibrations are determined by the UV-Vis and Fourier transform infrared (FTIR) and Raman (FTR) spectroscopy respectively. Information about particle size and morphological details of caped silver NPs is interpreted by transmission electron microscopy (TEM) followed by the selective area electron diffraction (SAED) techniques which give the patterns used to reveal the poly dispersion and size distribution nature.

***Key words*:** Ag nanoparticles, Antioxidant, Antibacterial, Heavy metal removal, Sonochemical

Nanomaterials have recently become one of the moist active research fields in the areas of solid-state physics, chemistry or engineer. These materials not only have potential applications as technological artifacts mechanical, optical, catalytic but also are of fundamental interest as the properties of a material which can drastically change between the macroscopic (bulk materials) and modular (aggregates) scales. On the other hand, the layer increase of the surface over volume ratio of the material induces drastic modifications of its diffusion properties (heterogeneous precipitation, grain boundaries segregation) [1].

* **A. Ayeshamariam**
✉ ayeshamariamkmc@gmail.com

[1-4] Department of Chemistry, Khadir Mohideen College (Bharathidasan University), Adirampattinam - 614 701, Tamil Nadu, India

[5] P. G. and Research Department of Physics, Thiagarajar College, Madurai - 625 009, Tamil Nadu, India

[6] Department of Physics, Khadir Mohideen College (Bharathidasan University), Adirampattinam - 614 701, Tamil Nadu, India

Silver has been valued throughout history for many of its properties that are useful to humans. It is used as a precious commodity in currencies, ornaments, jewelry, electrical contacts and photography, among others. One of the most beneficial uses of silver has been as a potent antibacterial agent that is toxic to fungi, viruses and algae. Silver has long been used as a disinfectant; for example, the metal has been used in treating wounds and burns because of its broad-spectrum toxicity to bacteria as well as because of its reputation of limited toxicity to humans [2].

Development of new nanomaterials with metal nanoparticles (Ag, Au, Cu, Rh, Pd, etc.) and its dopant, have gained much attention in material science because of expanding applications of such composites in optics, medical diagnostics, analytical chemistry, catalysis, photocatalysis etc. Silver crystallize in various types of crystal structures, leading to a variety of interesting physicochemical properties such as catalytic, electrochemical, electronic and optical properties. The samples were annealed in a furnace for one hour at 100, 150 and 200°C in air. XRD spectrum of the sample was recorded by means of PAN analytical X-ray diffractometer. A double beam spectrophotometer (Schimadzu 160A) was used for recording the UV/Vis spectrum. The optical behaviour displayed by materials such as selective absorption or reflection of different parts of the visible spectrum in the natural and artificial colours of everyday objects, can be thought of merely

as a special case of the response of a solid to the application of electric and magnetic field contained in the electromagnetic wave – the light. This selectivity naturally extends beyond the range of wavelengths we can see into both the ultra violet and the infrared parts of the electromagnetic spectrum in which the difference comes due to the electric field strength, changing alternatively in sign and amplitude at a very high frequency ranging between 1014 and 1016 Hz corresponding to wavelengths ranging from the infrared to the ultraviolet [3].

As the frequency of the incoming wave is raised and approaches the natural frequency of vibration of the lattice, the amplitude of the induced nuclear motion increases and the energy absorbed increases correspondingly reaching a maximum at the natural or resonant frequency. Beyond that frequency, the induced motion and energy absorption decrease due to the inertia of the nuclei. An optical wave of frequency substantially above the resonance frequency is transmitted with very little absorption of the lattice if the quantum of energy hυ is below the threshold for exciting transitions of the electrons between allowed energy levels. Thus, in insulators and semiconductors with a band gap in the electronic energy bands which is greater than the photon energy, the free electrons can be neglected in discussing the infrared spectra and can obtain information on crystal lattice absorption alone. In metals and very narrow band gap semiconductors, however the electrons dominate even in the infrared region [4].

The absorption and scattering of ultraviolet and visible radiations on the other hand is primarily due to the excitation of electrons into higher energy levels although nuclear motion as often can influence the effects that is observed. Hence the study of absorbed or emitted radiation as a function of wavelength is a powerful tool for the material scientists to use in characterizing solids, liquids and gases. The electronic energy levels which can thus be studied are not only a characteristic of the lattice and even the ionic species present, but also contain information about the immediate surroundings in which the atoms are situated. This could be understood if we recognize that (a) the number of occupied energy levels depend on the state of ionization of an atom and (b) the solutions to Schrodinger's equation must be slightly altered if the potential distribution in and around the nucleus is modified by the presence of neighboring ions [5].

MATERIALS AND METHODS

The *Cassia auriculata* (Fig 1) leaf was collected, washed, cut into small pieces and dried at room temperature (28±1°C) for two weeks and made into fine powder for further analysis. The shade-dried leaf powder of *Cassia auriculata* were subjected to extraction with 70% ethanol under reflux for 8 h and concentrated to a semisolid mass under reduced pressure (Rotavapor apparatus, Buchi Labortechnik AG, Switzerland). A dark semisolid (greenish-black) material was obtained and the yield was about 24% (w/w). It was stored at 4°C until used. When needed, the residual extract was suspended in distilled water and used for the study. The air dried, powdered plant material was extracted with petroleum ether, chloroform, alcohol, acetone-water and water separately in a conical flask at a room temperature. The total ash obtained from 2 gm of leaves powder was boiled for 5 minutes with 25 ml of dilute hydrochloric acid and the insoluble matter was collected on an ashless filter paper [6]. It was washed with hot water, ignited and weighed. 2 gm of *Cassia auriculata* leaf powder was taken in a tarred glass bottle and initial weight was taken. The sample was heated at 105°C in an oven and weighed. Ultraviolet–visible–near infrared (UV–Vis–NIR) spectra were carried out in the range of 200–800 nm using JASCO UV–Vis-NIR (Model-V-670) spectrophotometer. Bubble collapse leads to extreme temperatures (5000 – 50000 K), and pressure (100 atm) within the bubble. Solvent or solute molecules present within the bubbles are decomposed under these extreme conditions and generate highly reactive radicals.

Ag nanoparticles prepared in aqueous solution at 1 MHz

$H_2O \rightarrow H + OH$

$Ag^+ + H \rightarrow Ag + H^+$

Fig 1 Preparation of Ag (Silver) derived by assisting *C. auriculata* leaf extract by biosynthesis method

Instrumentation techniques

UV-visible spectral analysis was done by using Double beam UV-visible spectrophotometer (specrtoscan UV-2600), with the revolution of 1nm between 300-700 nm. The fluorescence measurements were carried out on F-7000 FL spectrophotometer with the scan speed of 1200 nm/min. FTIR spectra were recorded by using Bruker FTIR spectrophotometer in the range of 400-4000 cm^{-1}. The dried powder of silver nanoparticles was analyzed by XRD Bruker D8 advance XRD at 2θ degrees. Scanning Electron Microscopy (SEM) was done using Quanta 200 FEG, Particle size and crystalline nature of nanoparticles was analyzed using Transmission electron microscopy (TEM - JEO2100). Cyclic voltammetric study was done by using CH silicone voltammetric analyzer model 604 E work station with three electrode systems [7].

Antioxidant activity

The ability of the samples to annihilate the DPPH radical (1, 1-diphenyl-2-picrylhydrazyl) was investigated by the method described by (Blois 1958). Stock solution of compound was prepared to the concentration of 10 mg/ml. Different concentration of the extract (200, 400, 600, 800, 1000 µg) of sample were added, at an equal volume to methanolic solution of DPPH (0.1mM). The reaction mixture is incubated for 30 min at room temperature; the absorbance was recorded at 517 nm. The experiment was repeated for three times. Ascorbic acid was used as standard control. The annihilation activity of free radicals was calculated in percentage inhibition according to the following formula [8].

$$\text{Percent of inhibition} = \frac{\text{Absorbance of control} - \text{Absorbance of test}}{\text{Absorbance of control}} \times 100$$

Antibacterial Activity

Gram-Positive *Staphylococcus Aureus* (MTCC 96) bacterial pathogens were used for antimicrobial activity. These selected pathogenic strains were obtained from Microbial Type Culture Collection (MTCC), Chandigarh, and Punjab, India. The antibacterial activity was determined by well diffusion methods [9]. The streptomycin added well served as positive control. The solvent alone served as negative control. The plates were incubated at 37 °C in a 40 W florescent light source (~ 400 nm) for 24 hrs. The antibacterial activity was determined by measuring the diameter of the zone of inhibition around the well using antibiotic zone scale (Himedia, Mumbai, India) [10].

RESULTS AND DISCUSSION

Structural characterization

As for as concern the structural investigation on nanopowder the PXRD is very important techniques to full width at the half maximum of the peak, resemblance to crystalline peak orientations, lattice and geometrical constants, identification of purity among intensities of peaks, preferred Orientation as well as defects and stresses, etc. The crystal lattice presents a series of parallel reflecting planes to the incident x-ray beam. The intensity of the reflected beam at certain angles will be maximum when the path difference between two reflected waves from two different crystal planes is an integral multiple of λ. This condition is termed as Bragg's law and is given by, nλ = 2d Sinθ, where, n is the order of diffraction, λ is the wavelength of x-rays, d is the spacing between consecutive parallel planes and θ is the glancing angle (or the complement of the angle of incidence) [11].

The lattice parameter *c* of the as-deposited room temperature silver nanoparticle is calculated using the formula for the hexagonal crystal structure. For the cubic crystal system, the lattice parameter a is related to *d* with the following equation:

$$\frac{1}{d^2} = \frac{h^2 + k^2 + l^2}{a^2}$$

Where *h*, *k*, and *l* are all integers, *(hkl)* is the lattice plane index, *a* is a lattice constant, d_{hkl} is distance between two consecutive planes (m=1) with lattice plane index *(hkl)*. To determine the micro structural detail of the film, X-ray diffraction analysis was conducted using X'pert PRO (PANalytical) diffractometer with CuKα radiation and employing a scanning rate of 5° min^{-1}.

Utilizing the X-ray diffraction data, the average particle/grain size in Ag was estimated by Scherrer's equation, Crystallite size D = kλ/ β scosθ (nm), where D is grain size, β the full width at half maxima and λ the wavelength of X-ray used (1·5409 Å). The crystallite size and thickness of different annealing temperatures values are plotted in (Fig 2).

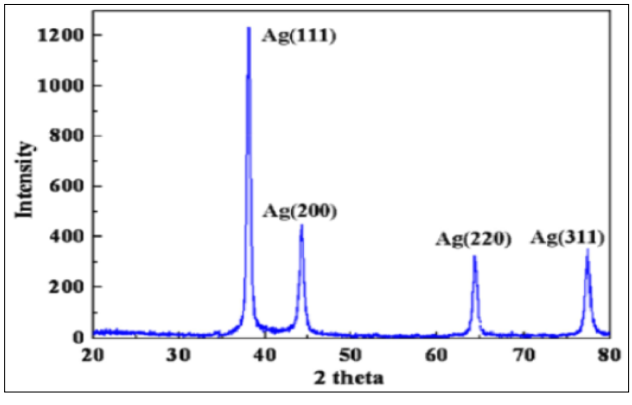

Fig 2 Powder X-ray diffractometry (XRD) of Ag nanoparticles and the position of the diffraction peaks

Table 1 XRD (Structural) parameters of Ag asprepared NPs

Sample	Position (2θ)	(hkl)	a Å	Crystalline size (nm)	Strain (β cos θ/4)
Asprepared	38.431	111	4.0692	31.522	0.000948
89-3722	44.530	200	4.0702	29.255	0.000459
(JCPDS)	64.525	220	4.0895	25.252	0.000412

It can be clearly seen as shown in the (Fig 2), the diffraction pattern of the Ag NPs corresponds to a crystal system with characteristic diffraction peaks, there are three distinct diffraction peaks at 2θ values of 38.043°, 44.530° and 64.525° can be indexed to the (111), (200) and (220) reflection planes of face-centered cubic structure of silver nano particles respectively as per the JCPDS-ICDD Ref. C. No. 89-3722. It reveals that the slight shift from the standard data in the peaks indicates that the overall resulting action of capping as well as size reducing agents of entitled herbal extract on the obtained Ag NPs was confirmed through the PXRD analysis. It shows that that although the results from PXRD are in good agreement with those, in the SAED pattern, since the first one gives us more significant information while the diffraction is performed on a group of particles, the scanned area in PXRD is much larger [12].

TEM and SAED analysis

The transmission electron microscope with spatial high resolving power and analytical information was used to elucidate the quantitative observation of particles nature, size distribution, structure and morphology of the obtained Ag NPs. The optical zoom of TEM was observed as the ratio of object distance from the sample to the image distance from objective lens in the range of 20 nm and 10 nm magnification as shown in the (Fig 3a-b), respectively. Among all zone of the images shows the each and every particles scale ranging from higher nano dimension to lowers are crystalline as shown in the both observed images which reveals the polycrystalline NPs as well as this image 3 (b) and size distributions of Ag NPs showed that the mean diameter of the nanoparticles ranged from about 30 to 10 nm confirms the face-centered cubic (FCC) crystalline structure of Ag NPs with negligible particle agglomeration and dispersion [13].

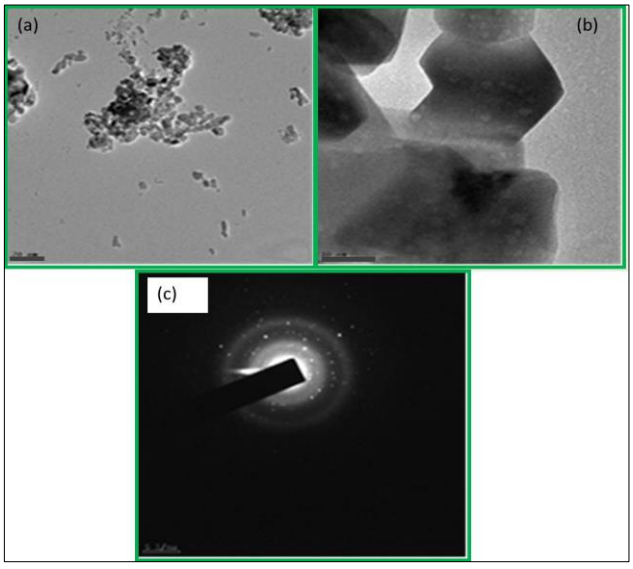

Fig 3 a-b Transmission electron microscopy (TEM) images of Ag crystalline nanoparticles (c) Selected area electron diffraction (SAED) pattern

In order to investigate the crystallography parameter like crystalline phase and structure of the green synthesized sample,

elucidated SAED pattern was observed on many zone of particles cluster, as shown in Figure 3 (c). Determination of phases was inferred by matching with the corresponding diffraction patterns from the JCPDS: ICDD (89-3722) international diffraction database [14].

UV-Vis or DRS UV Spectroscopy

The UV–Visible optical absorption spectrum of the green synthesized Ag NPs out at room temperature using UV Visible spectrometer (Model: Shimadzu -1700 series) from 200 to 800 nm and are shown in (Fig 4a). The absorption spectra infers the details of absorption of the illuminated light on the sample and strong absorption observed at ~ 410 nm considered as higher absorption whereas the transmission spectra of the Ag nanoparticles shows just reverse seen of curve of the optical absorption spectra. The optical band gap was calculated and plotted between bandgap energy in eV and $(\alpha h\nu)^2$ using the Tauc relation $\alpha = A(h\nu - E_g)^{1/2}$, where α, h, ν, A, and E_g are the absorption coefficient, Plank's constant, frequency of photons, value of absorption in arbitrary unit and band gap in eV respectively. The band gap curve as shown in the (Fig 4) depicted as per the variation of $(\alpha h\nu)^{1/n}$ vs. photon energy (hν) with n = 1/2, direct allowed transition band gap of Ag NPs and calculated to be 3.39 eV, which is closer to the reported value 3.2101 eV [15].

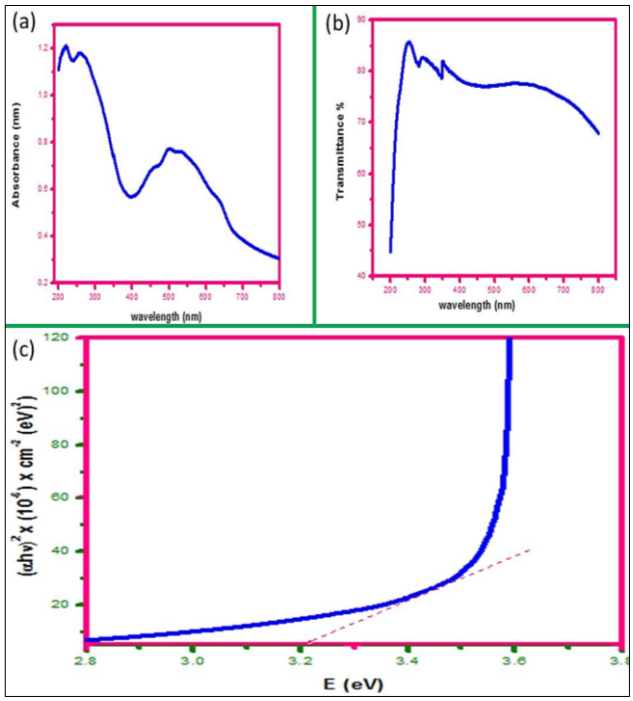

Fig 4 (a) UV–Visible absorption spectra (b) UV–Visible transmittance spectra of green synthesized silver nanoparticles as a function of wavelength. (c) The $(\boldsymbol{\alpha}h\boldsymbol{\upsilon})^2$ versus $h\boldsymbol{\upsilon}$ curves for the optical band gap determination of green synthesized silver nanoparticles

FTIR analysis

FTIR is an effective technique to measure and carry out the identification major functional groups in the leaf extract and their possible capping action involvement in the synthesis and stabilization of Ag NPs. The spectrum of green synthesized Ag nano powder sample under the IR environment is represented in (Fig 5). Due to the presence of leaf compositions, it showed several peaks instead of single nosedive indicating the complex nature of the phytomaterial. The bands appearing at 3419, 2501, 1654, 1084, and 510 cm^{-1} were assigned to stretching vibration of OH stretching, C-H stretching, C-C stretching, C-H bending, C-Ag vibrations respectively. There were some shifts in the peaks against the standard known values of synthesized Ag Nps which reveals that confirmation of functional groups of leaf extract participate as a capping agent in the formation of Ag NPs [16].

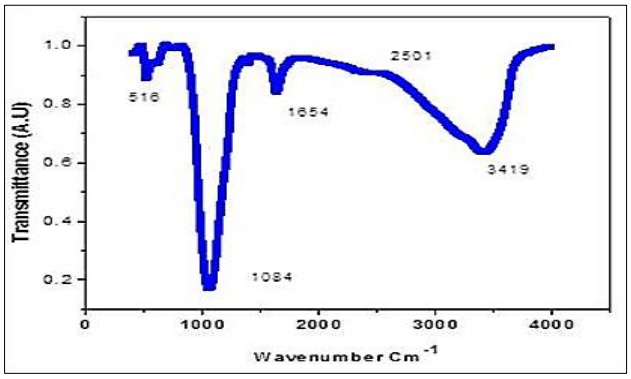

Fig 5 FTIR Analysis of Ag nanoparticles

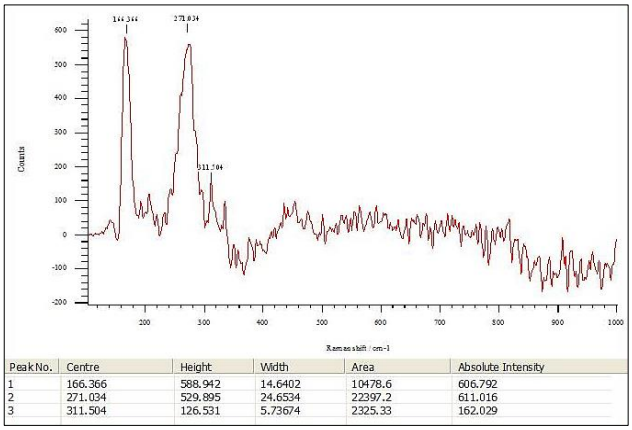

Peak No.	Centre	Height	Width	Area	Absolute Intensity
1	166.366	588.942	14.6402	10478.6	606.792
2	271.034	529.895	24.6534	22397.2	611.016
3	311.504	126.531	5.73674	2325.33	162.029

Fig 6 Laser Raman analysis of Ag NPs

Laser Raman analysis

Raman spectroscopy is a useful technique to characterize the structure and quality of Ag NPs. In particular, it is effective in determining the defects and disordered and ordered characteristics of Nanoparticles. Since both IR and Raman spectrum are complement to each other, the some peaks what is not there is here. That observed peaks 166.37 $cm^{-1,}$ 271.03 and 311.5 cm^{-1} confirm the presence of alkyl silver functional groups shown in (Fig 6) [17].

Antioxidant properties of Ag NPs against DPPH

In the present study, the DPPH free-radical scavenging potential of *C. auriculata* leaf aqueous extract and Ag NPs in a wide range of concentrations revealed impressive prevention similar to that of BHT as a standard antioxidant agent. Free-radicals are molecules that do not have a complete electron shell and are capable of increasing the chemical reaction compared to others. They are formed if the human body is exposed to tobacco smoke and radiation. In humans, the most important free radical is oxygen. When an oxygen molecule (O_2) is exposed to radiation, it removes an electron from the other molecules, destroying DNA and other molecules. Some of these changes may cause a number of persistent diseases, e.g., heart problems, muscle failure, diabetes and cancer [18]. Antioxidants act like a broom against free radicals and have been recognized as powerful remedies to destroy free radicals and regenerate the damaged cells. More importantly, laboratory evidence has shown that antioxidants can highly prevent cancer [19]. The IC_{50} of *C. auriculata* leaf aqueous extract, BHT, and

Ag NPs were 312, 201, and 185 µg/mL, respectively (Table 1). Metallic nanoparticles have also excellent potential to inhibit DPPH. The results obtained in our study are in line with many studies in which the mutual effect has been monitored to increase the antioxidant capacities between herbs and metallic salts against DPPH [20].

In general, metallic nanoparticles display remarkable and extraordinary antioxidant impacts, among which the antioxidant effects of Ag NPs have been well-documented. When Ag NPs are synthesized with medicinal plants, the Fe element forms a very strong bond with flavonoid and phenolic compounds, creating unique antioxidant effects. In a previous study, it was indicated that *C. auriculata* NPs is a rich source of antioxidant compounds including terpenoids compounds which were formerly mentioned. Several studies were carried out in the nanotechnology field using various medicinal plants, but to the best of our knowledge, no report is available on Ag NPs synthesized using *C. auriculata* NPs leaf aqueous extract [21].

Table 2 The IC50 of Ag NPs, *C. auriculata* leaf aqueous extract, *C. auriculata* NPs, and BHT in antioxidant test

Sample	Ag NPs (µg/mL)	*C. auriculata* leaf	Ag NPs (µg/mL)	BHT (µg/mL)
IC_{50} against DPPH	-	312 ± 0^{b}	185 ± 0^{b}	201 ± 0^{b}

Antibacterial studies

Gram-positive *Staphylococcus Aureus* (MTCC 96) bacterial pathogens were used for antimicrobial activity. The antibacterial activity of synthesized antioxidant towards Gram-positive (*S. aureus*) was investigated by well diffusion method. (Fig 7) shows the photographic images which depict the inhibition zones formed around the well. From the picture, it is found that the diameter of the zone of inhibition is larger for green synthesized caped Ag NPs sample for 5mg/ml compared with positive control as shown in the (Table 2) [22].

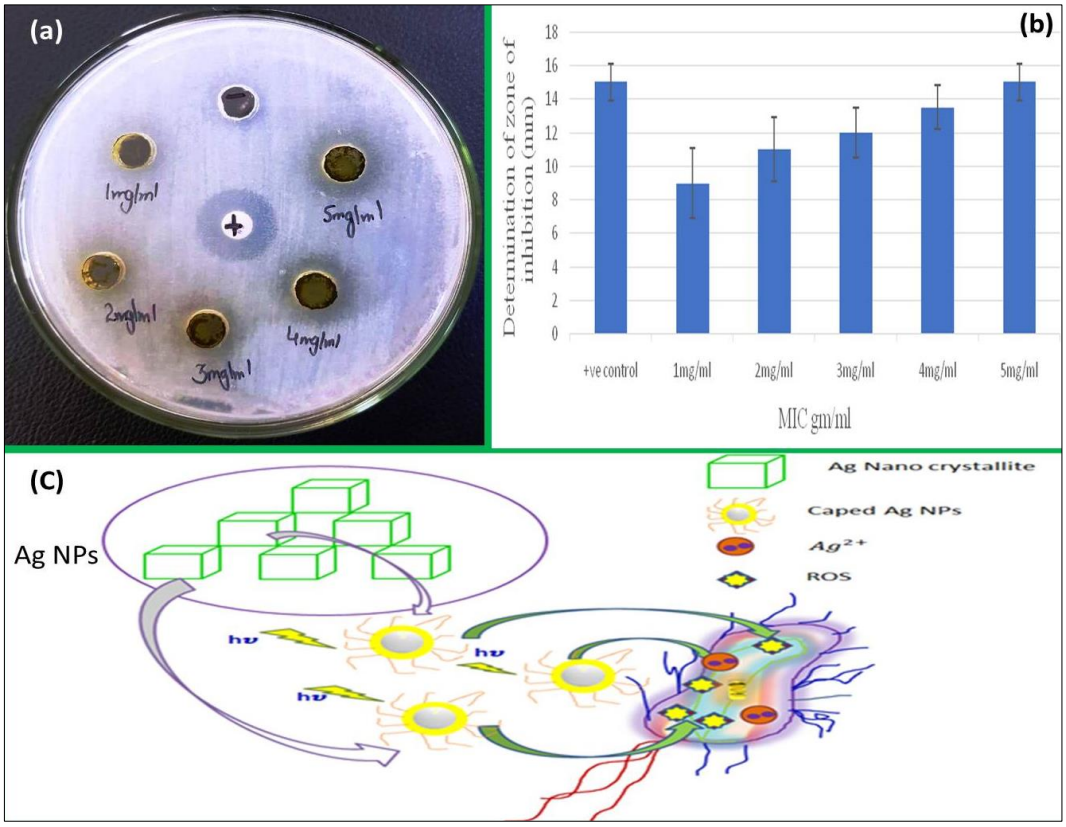

Fig 7(a) Photographic images which depict the inhibition zones formed around the well 7(b) Ejection of Ag^{2+} ions from the caped silver NPs (c) structure, size and shape of the prepared sample 7(c) Four chem-bio parameters involved in the proposed mechanism of antibacterial activity

This variation tells that samples at various concentration exhibits higher antibacterial efficiency towards gram-positive bacteria. Four chem-bio parameters involved in the proposed mechanism of antibacterial activity as shown in the (Fig 7c) are listed as follows, (Fig 7a) generation of reactive oxygen species as well as the formation of super ion entities (Fig 7b) Ejection of Ag^{2+} ions from the caped silver NPs (c) structure, size and shape of the prepared sample. When electromagnetic waves with adequate photon energy are incident on bio culture environment associated with sample, excitons are formed leads to generation of ROS itself. The electromagnetic interaction with sample provides the more oxidative stress than stress limit on the microbes due to the action of photo-exciton ROS can be perturbed the cell wall, nucleus, membrane, proteins and DNA promoting the cell damage. The super-radicals interaction with cell walls and dissociates it for easy entering or penetrating into the cell domain. The crucial function of ROS is remarkable one in the antibacterial activity of entitled sample. From the TEM studies, it is found that the larger S/V of particles is a crucial key role in zone of inhibition leads to excellence of potential in antibacterial actions for certain excellent pharmaceutical candidates [23].

CONCLUSION

Ag nanoparticles have been successfully synthesized by a Sonochemical method by accompanying the *C. auriculata* herbal leaf extract. The PXRD and TEM with SAED data outcomes revealed the cubic structure without any additional phase of impurities, particles dimension and morphology. The

presence of functional groups of phytochemicals and the chemical bonding with Ag are confirmed by FTIR and Laser Raman spectra. This optimized silver nanoparticle reveals good antimicrobial activity against gram positive staphylococcus aureus from the detailed investigation. So, the prepared green synthesized Ag NPs nanoparticles have found applications in biomedical and pharmaceutical flat form as well as water purification processes for inhibiting the growth of bacteria.

LITERATURE CITED

1. Gao YZ, Chang TX, Wu YX. 2019. In-situ preparation and properties of bio-renewable acylated sodium alginate-g-polytetrahydrofuran/Ag-NPs nanocomposites. *Applied Surface Science* 483: 1027-1036.
2. Senthilkumar P, Yaswant G, Kavitha S, Chandramohan E, Kowsalya G, Vijay R, Sudhagar B, Kumar DRS. 2019. Preparation and characterization of hybrid chitosan-silver nanoparticles (Chi-Ag NPs); A potential antibacterial agent. *International Journal of Biological Macromolecules* 141: 290-298.
3. Oun AA, Rhim JW. 2017. Preparation of multifunctional chitin nanowhiskers/ZnO-Ag NPs and their effect on the properties of carboxymethyl cellulose-based nanocomposite film. *Carbohydrate Polymers* 169: 467-479.
4. Zayed MF, Eisa WH, Abdel-Moneam YK, El-Kousy SM, Atia A. 2015. Ziziphus spina-christi based bio-synthesis of Ag nanoparticles. *Journal of Industrial and Engineering Chemistry* 23: 50-56.
5. Duan C, Liu C, Meng X, Gao K, Lu W, Zhang Y, Dai L, Zhao W, Xiong C, Wang W, Liu Y. 2020. Facile synthesis of Ag NPs@ MIL-100 (Fe)/guar gum hybrid hydrogel as a versatile photocatalyst for wastewater remediation: Photocatalytic degradation, water/oil separation and bacterial inactivation. *Carbohydrate Polymers* 230: 115642.
6. Yazdi MET, Khara J, Housaindokht MR, Sadeghnia HR, Bahabadi SE, Amiri MS, Mosawee H, Taherzadeh D, Darroudi M. 2019. Role of ribes khorassanicum in the biosynthesis of AgNPs and their antibacterial properties. *IET Nanobiotechnology* 13(2): 189-192.
7. Rehan M, Mowafi S, Aly SA, Elshemy NS, Haggag K. 2017. Microwave-heating for in-situ Ag NPs preparation into viscose fibers. *European Polymer Journal* 86: 68-84.
8. Yang J, An X, Liu L, Seta FT, Zhang H, Nie S, Yao S, Cao H, Xu Q, Liu H, Ni Y. 2020. Chitin nano-crystals/sodium lignosulfonate/Ag NPs nanocomposites: a potent and green catalyst for efficient removal of organic contaminants. *Cellulose* 27(9): 5071-5087.
9. Luo S, Fan L, Yang K, Zhong Z, Wu X, Ren T. 2018. In situ and controllable synthesis of Ag NPs in tannic acid-based hyperbranched waterborne polyurethanes to prepare antibacterial polyurethanes/Ag NPs composites. *RSC Advances* 8(64): 36571-36578.
9. El-Nahrawy AM, Ali AI, Abou Hammad AB, Youssef AM. 2016. Influences of Ag-NPs doping chitosan/calcium silicate nanocomposites for optical and antibacterial activity. *International Journal of Biological Macromolecules* 93: 267-275.
10. Youssef AM, Hasanin MS, Abd El-Aziz ME, Turky GM. 2021. Conducting chitosan/hydroxylethyl cellulose/polyaniline bionanocomposites hydrogel based on graphene oxide doped with Ag-NPs. *International Journal of Biological Macromolecules* 167: 1435-1444.
11. Tippayawat P, Phromviyo N, Boueroy P, Chompoosor A. 2016. Green synthesis of silver nanoparticles in aloe vera plant extract prepared by a hydrothermal method and their synergistic antibacterial activity. *Peer Journal* 4: p.e2589.
12. Senthilkumar P, Yaswant G, Kavitha S, Chandramohan E, Kowsalya G, Vijay R, Sudhagar B, Kumar DRS. 2019. Preparation and characterization of hybrid chitosan-silver nanoparticles (Chi-Ag NPs); A potential antibacterial agent. *International Journal of Biological Macromolecules* 141: 290-298.
13. Divya M, Kiran GS, Hassan S, Selvin J. 2019. Biogenic synthesis and effect of silver nanoparticles (AgNPs) to combat catheter-related urinary tract infections. *Biocatalysis and Agricultural Biotechnology* 18: 101037.
14. Ren S, Zhao G, Wang Y, Wang B, Wang Q. 2015. Enhanced photocatalytic performance of sandwiched ZnO@ Ag@ Cu_2O nanorod films: the distinct role of Ag NPs in the visible light and UV region. *Nanotechnology* 26(12): 125403.
15. Sikder M, Lead JR, Chandler GT, Baalousha M. 2018. A rapid approach for measuring silver nanoparticle concentration and dissolution in seawater by UV–Vis. *Science of the Total Environment* 618: 597-607.
16. Yang Y, Luo L, Li HP, Wang Q, Yang ZG, Long CL. 2016. Separation and determination of silver nanoparticle in environmental water and the UV-induced photochemical transformations study of AgNPs by cloud point extraction combined ICP-MS. *Talanta* 161: 342-349.
17. Jayaprakash N, Vijaya JJ, Kaviyarasu K, Kombaiah K, Kennedy LJ, Ramalingam RJ, Munusamy MA, Al-Lohedan HA. 2017. Green synthesis of Ag nanoparticles using Tamarind fruit extract for the antibacterial studies. *Journal of Photochemistry and Photobiology B: Biology* 169: 178-185.
18. Raza MA, Kanwal Z, Rauf A, Sabri AN, Riaz S, Naseem S. 2016. Size-and shape-dependent antibacterial studies of silver nanoparticles synthesized by wet chemical routes. *Nanomaterials* 6(4): 74.
19. Das G, Patra JK, Shin HS. 2020. Biosynthesis, and potential effect of fern mediated biocompatible silver nanoparticles by cytotoxicity, antidiabetic, antioxidant and antibacterial, studies. *Materials Science and Engineering: C* 114: 111011.
20. Chandhru M, Logesh R, Rani SK, Ahmed N, Vasimalai N. 2019. One-pot green route synthesis of silver nanoparticles from jack fruit seeds and their antibacterial activities with *Escherichia coli* and salmonella bacteria. *Biocatalysis and Agricultural Biotechnology* 20: 101241.
21. Majeed S, Danish M, Zahrudin AHB, Dash GK. 2018. Biosynthesis and characterization of silver nanoparticles from fungal species and its antibacterial and anticancer effect. *Karbala International Journal of Modern Science* 4(1): 86-92.
22. Gopinath PM, Narchonai G, Dhanasekaran D, Ranjani A, Thajuddin N. 2015. Mycosynthesis, characterization and antibacterial properties of AgNPs against multidrug resistant (MDR) bacterial pathogens of female infertility cases. *Asian Journal of Pharmaceutical Sciences* 10(2): 138-145.
23. Jaiswal S, Duffy B, Jaiswal AK, Stobie N, McHale P. 2010. Enhancement of the antibacterial properties of silver nanoparticles using β-cyclodextrin as a capping agent. *International Journal of Antimicrobial Agents* 36(3): 280-283.